

# Bromination of 2D materials

Eva Marie Freiberger<sup>1,5</sup> , Julien Steffen<sup>2,5</sup> , Natalie J Waleska-Wellenhofer<sup>1</sup> ,  
Felix Hemauer<sup>1</sup> , Valentin Schwaab<sup>1</sup> , Andreas Görling<sup>2,3</sup> ,  
Hans-Peter Steinrück<sup>1</sup>  and Christian Papp<sup>1,4,\*</sup> 

<sup>1</sup>Physikalische Chemie II, Friedrich-Alexander-Universität Erlangen-Nürnberg, Egerlandstr. 3, D-91058 Erlangen, Germany

<sup>2</sup>Theoretische Chemie, Friedrich-Alexander-Universität Erlangen-Nürnberg, Egerlandstr. 3, D-91058 Erlangen, Germany

<sup>3</sup>Erlangen National High Performance Computing Center (NHR@FAU), Martensstr. 1, D-91058 Erlangen, Germany

<sup>4</sup>Physikalische und Theoretische Chemie, Freie Universität Berlin, Arnimallee 22, D-14195 Berlin, Germany

E-mail: [christian.papp@fau.de](mailto:christian.papp@fau.de)

Received 19 July 2023, revised 7 November 2023

Accepted for publication 30 November 2023

Published 17 January 2024



CrossMark

## Abstract

The adsorption, reaction and thermal stability of bromine on Rh(111)-supported hexagonal boron nitride (*h*-BN) and graphene were investigated. Synchrotron radiation-based high-resolution x-ray photoelectron spectroscopy (XPS) and temperature-programmed XPS allowed us to follow the adsorption process and the thermal evolution *in situ* on the molecular scale. On *h*-BN/Rh(111), bromine adsorbs exclusively in the pores of the nanomesh while we observe no such selectivity for graphene/Rh(111). Upon heating, bromine undergoes an on-surface reaction on *h*-BN to form polybromides (170–240 K), which subsequently decompose to bromide (240–640 K). The high thermal stability of Br/*h*-BN/Rh(111) suggests strong/covalent bonding. Bromine on graphene/Rh(111), on the other hand, reveals no distinct reactivity except for intercalation of small amounts of bromine underneath the 2D layer at high temperatures. In both cases, adsorption is reversible upon heating. Our experiments are supported by a comprehensive theoretical study. DFT calculations were used to describe the nature of the *h*-BN nanomesh and the graphene moiré in detail and to study the adsorption energetics and substrate interaction of bromine. In addition, the adsorption of bromine on *h*-BN/Rh(111) was simulated by molecular dynamics using a machine-learning force field.

Supplementary material for this article is available [online](#)

Keywords: hexagonal boron nitride, graphene, bromine, functionalization, x-ray photoelectron spectroscopy, molecular dynamics, machine-learning force field

## Introduction

In recent years, two-dimensional materials (2DM) have become a flourishing research field due to their unique

properties, rendering them promising candidates for various applications. Since 2004, when Novoselov *et al* reported on the first successful isolation of graphene [1], a plethora of different 2DM has been theoretically predicted, synthesized and characterized. Up to now, the family of 2DM comprises numerous homonuclear graphene analogs, e.g. phosphorene, borophene, silicene and germanene [2–5], and heteronuclear members, such as hexagonal boron nitride (*h*-BN) and transition metal dichalcogenides [6, 7]. Out of these, graphene, which is built up from sp<sup>2</sup>-hybridized carbon atoms arranged in a honeycomb pattern [8], is by far the most studied 2DM. This intensive research effort is motivated by its

<sup>5</sup> The authors contributed equally to this work.

\* Author to whom any correspondence should be addressed.



Original content from this work may be used under the terms of the [Creative Commons Attribution 4.0 licence](#). Any further distribution of this work must maintain attribution to the author(s) and the title of the work, journal citation and DOI.

startling chemical, electronic and mechanical properties. Graphene is a zero-bandgap semiconductor, showing a high charge carrier mobility and good thermal conductivity [9–11], which makes it interesting for the development of micro-electronic devices. However, opening its bandgap would be a prerequisite for any application in this field. In addition to its unique electronic properties, graphene is chemically and mechanically quite robust and optically transparent [12, 13]. This renders it promising for the design of optoelectronic devices, such as advanced solar cells [14, 15]. Hydrogenated graphene has even been investigated as a possible hydrogen carrier, enabling chemical energy storage [16]. An overview of graphene research is given in many comprehensive review articles, reporting on the different preparation methods and the manifold properties and applications [17–20]. Another well-studied 2DM is *h*-BN, a structural graphene analog, consisting of alternating boron and nitrogen atoms. *h*-BN has a large bandgap of  $\sim 6$  eV and may hence be utilized as a dielectric layer in microelectronic devices, e.g. as a 2D substrate for graphene [21]. It also shows remarkable chemical inertness and thermal stability, which render *h*-BN, for example, suitable as a protective coating [22, 23]. As in the case of graphene, detailed information about the synthesis, properties and applications of *h*-BN is provided in literature [24, 25].

Ultra-high vacuum (UHV) provides a clean and controlled environment, allowing for an understanding of chemical processes on the molecular level. In UHV, graphene and *h*-BN can be prepared *in situ* by chemical vapor deposition (CVD) of a precursor molecule on a hot single-crystal surface acting as the support. In general, these supported 2DM show different properties compared to the free-standing 2DM as they interact with the respective substrate. The support has a significant impact on the morphology of the 2D layers: if *h*-BN or graphene are grown on a lattice-mismatched substrate, buckling of the 2DM takes place, leading to a so-called moiré pattern with pores/valleys (strong interaction with the substrate) and wires/hills (weak interaction with the substrate) [26, 27]. For graphene or *h*-BN growth on a Rh(111) substrate, such a corrugation occurs [6, 28], which is in the case of *h*-BN/Rh(111) referred to as nanomesh. The *h*-BN nanomesh and the graphene moiré can be used as templates for spatially confined adsorption of atoms, molecules or metal clusters [29, 30].

To tune the intrinsic properties of supported 2DM towards specific applications, their chemical modification is subject to intensive research. In literature, many examples of the successful synthesis of graphene derivatives can be found, from early attempts to prepare graphene oxide to recent studies on functionalized graphene as a promising electrode material for advanced energy storage devices, such as supercapacitors [31–33]. However, most of these examples rely on wet-chemical preparation methods and are thus not applicable in a pure UHV approach, which is key to mechanistic understanding of the growth and modification of 2DM. In UHV, several strategies can be applied to achieve chemical modification of 2DM, e.g. doping with heteroatoms, such as boron (p dopant) and nitrogen (n dopant) [34, 35], or

intercalation [36, 37]. Also, the non-covalent and covalent functionalization of 2DM is a promising route towards distinct chemical modification. In this context, graphene functionalization with atomic hydrogen and oxygen has been reported [38, 39]. Despite of its chemical inertness, covalent functionalization of supported *h*-BN with atomic hydrogen and molecular oxygen has also been shown to be possible. Using Ni(111) as support, Späth *et al* observed covalent functionalization of the 2DM [40, 41]. The *h*-BN/Rh(111) nanomesh, on the other hand, allowed for spatially defined modification due to the different reactivity of the pores and wires [42]. Besides hydrogen and oxygen, halogens may be suitable candidates for the functionalization of 2DM as they are quite reactive and thus are expected to have a significant impact on the electronic structure. Furthermore, the halogenation of 2DM represents a good starting point for further functionalization, e.g. with small molecules, such as pyridine or ammonia [43].

Here, we present a state-of-the-art *in situ* surface science study with the main goal to elucidate the adsorption process, reactivity and thermal stability of bromine on Rh(111)-supported *h*-BN and graphene. High-resolution x-ray photoelectron spectroscopy (XPS) and temperature-programmed XPS (TPXPS) were employed to gain detailed information regarding the adsorption process, the thermally induced on-surface reaction and the thermal stability of adsorbed bromine. In addition, a comprehensive theoretical study was performed to complement the experiments.

Our work provides a thorough investigation of the chemical reactivity of Rh(111)-supported, corrugated *h*-BN and graphene towards bromine. In the case of the *h*-BN/Rh(111) nanomesh, we even achieved controlled lateral chemical modification, i.e. covalent functionalization in the pores. We attribute this to a laterally different electronic structure and reactivity of the nanomesh, which is the prerequisite for any lateral structuring via covalent functionalization. Our findings also encourage further microscopic investigations to elucidate the structure in detail. The new fundamental insights gained within this study expand the understanding of these systems on the molecular level and lay the foundation for purposeful tailoring of the properties of 2DM.

## Experimental methods and computational details

To investigate the adsorption and thermal stability of bromine on *h*-BN/Rh(111) and graphene/Rh(111) *in situ*, we performed synchrotron radiation-based high-resolution XPS and TPXPS. The experiments were conducted at the open port undulator beamlines UE56/2-PGM 2 and U49/2-PGM 1 [44] at the electron storage ring BESSY II of the Helmholtz Zentrum Berlin (HZB). Our transportable two-chamber UHV apparatus is described in detail elsewhere [45]. It is, *inter alia*, equipped with a hemispherical electron energy analyzer, a supersonic molecular beam and a microcapillary array dosing system. The latter allows for dosing bromine directly into the analyzer chamber. Our setup enables cooling of the sample to approximately 100 K using liquid nitrogen as well as heating,

either resistively up to 1400 K or by a tungsten filament mounted behind the sample up to about 550 K. The sample temperature is monitored by thermocouples (K type) spot-welded to the sample. All experiments were performed with a Rh(111) single crystal (MaTeck) as the substrate. Prior to sample preparation and measurements, its surface was cleaned by several cycles of Ar<sup>+</sup> sputtering, annealing to 1200 K and oxygen treatment at 900 K. Thereafter, the crystal was checked for impurities by XPS.

*h*-BN was grown on Rh(111) by dosing  $\sim 2 \times 10^{-8}$  mbar borazine, synthesized according to Sneddon [46], for about 40 min ( $T_{\text{Substrate}} = 1050$  K). Preparation of graphene was achieved by dosing  $\sim 1 \times 10^{-8}$  mbar ethylene for about 60 min ( $T_{\text{Substrate}} = 920$  K) using the molecular beam. The growth of *h*-BN and graphene was followed *in situ* by XPS to ensure good quality of the respective 2DM. Subsequently, the Rh(111)-supported 2DM were exposed to a background pressure of elemental bromine in the analyzer chamber ( $T_{\text{Substrate}} = 170$  K). This substrate temperature was chosen to avoid water contamination of the sample. The adsorption itself and the resulting modified 2DM were probed by XPS. Between each spectrum, the sample was shifted by about 0.1 mm (larger than the x-ray beam diameter) to avoid beam damage. Next, the thermal stability and reactivity of the adsorbed bromine was tested by TPXPS. To this end, XP spectra in the Br 3d region were continuously measured in intervals of about 10 K while the sample was heated to 550 K using the tungsten filament with a heating ramp of  $0.5 \text{ K s}^{-1}$ . For temperatures above 550 K, the filament was turned off and the sample was heated resistively (in 25–50 K steps).

All spectra were recorded in normal emission. The chosen photon energies were 170 eV for the Br 3d region (energy resolution: 210 meV), 280 eV for the B 1s region (290 meV), 380 eV for the C 1s (200 meV) and Rh 3d region (200 meV) and 500 eV for the N 1s region (250 meV). The binding energies were referenced with respect to the Fermi edge and a linear background was subtracted. Peak fitting was performed using a convolution of Gaussian and Doniach-Šunjić functions. The fit parameters are listed in table S1 in the supplementary information (SI). The exposure of bromine, calculated from the background pressure in the chamber and the exposure time, is given in Langmuir (L,  $1.33 \times 10^{-6}$  mbar s). The surface coverage is given in monolayers (ML), whereby 1 ML corresponds to one adsorbed atom per surface atom. For calibration of the bromine coverage, bromobenzene (C<sub>6</sub>H<sub>5</sub>Br) was used. C<sub>6</sub>H<sub>5</sub>Br was adsorbed on clean Rh(111), the resulting carbon coverage was determined by comparison to graphene/Rh(111) and therefrom the corresponding bromine signal was calibrated. All bromine coverages were then determined referring to this known C<sub>6</sub>H<sub>5</sub>Br coverage. Due to the lattice mismatch of *h*-BN on Rh(111),  $12 \times 12$  Rh(111) unit cells are covered with  $13 \times 13$  *h*-BN unit cells [47]. Thus, a single layer of *h*-BN corresponds to 1.17 ML nitrogen and 1.17 ML boron. These coverages were used to calibrate the N 1s and B 1s spectra. In analogy, the carbon coverage was determined referring to the graphene C 1s spectrum (Rh:G unit cell ratio = 11:12), which

corresponds to 2.38 ML carbon [27]. Regarding the coverage determination, we estimate an error of about  $\pm 0.02$  ML.

Periodic DFT calculations of the systems were carried out in the VASP code (version 6.3), in which a plane wave basis set for the description of the valence electrons is used in combination with the projector augmented wave (PAW) method for the representation of the atomic cores [48–50]. The kinetic energy cutoff was chosen to be 400 eV and exchange correlation effects were treated with the PBE functional [51]. The DFT-D3 correction was used for a better description of dispersion interactions [52, 53].

For *h*-BN on Rh(111), a full  $13 \times 13$  on  $12 \times 12$  nanomesh unit cell was modeled with a surface slab of three metal atom layers. The dimensions of the investigated structure measure  $32.27 \text{ \AA}$  along the *a*- and *b*-axes, and  $24 \text{ \AA}$  along the *c*-axis, leaving approximately  $16 \text{ \AA}$  of vacuum between the periodic images of the nanomesh. The structure of the *h*-BN nanomesh cell was obtained from the author of [54] and reoptimized with our settings until the largest cartesian force component was below  $0.03 \text{ eV \AA}^{-1}$ , which led to only small displacements of the atoms. The structure of the nanomesh and the topmost metal layer were optimized, while the lower two layers were kept fixed at the geometry of [54]. The  $12 \times 12$  on  $11 \times 11$  graphene moiré unit cell was modeled with a surface slab of three metal atom layers as well. The *a*- and *b*-axes are  $29.66 \text{ \AA}$  long and the *c*-axis measures  $25 \text{ \AA}$ . The initial structure of this cell was obtained from the authors of [55–58] and reoptimized from a four- to a three-metal-atom-layer model. The positions of the bromine atoms and molecules were optimized with the same settings, whereas only the positions of nanomesh/moiré atoms within a sphere of  $6 \text{ \AA}$  around any bromine atom were optimized. This approach was also applied when testing the desorption of bromine molecules. For more than four bromine molecules on the nanomesh, the maximum force criterion was difficult to meet. Instead, a total energy change of less than  $10^{-5} \text{ eV}$  was chosen as the convergence criterion.

Due to the large size of the system (770 atoms without bromine for *h*-BN, 651 for graphene), Brillouin zone sampling was restricted to the Gamma point during geometry optimizations while, for core level shift and band structure calculations, a Gamma-containing  $3 \times 3 \times 1$  k-point mesh was chosen. A first-order Methfessel–Paxton scheme with a broadening of 0.1 eV was applied to smear the electronic states [59].

For the generation of the reactive force field (FF), describing the interaction of bromine with *h*-BN on Rh(111), the VASP machine-learning FF was used [60–62]. Using the whole nanomesh unit cell for machine-learning molecular dynamics (MD) would have been computationally too expensive. Instead, the three model surfaces well known from literature, top/hcp, fcc/top and hcp/fcc ( $5 \times 5$  on  $5 \times 5$  nanomesh,  $12.71 \text{ \AA}$  along the *a*- and *b*-axes and  $27.06 \text{ \AA}$  along the *c*-axis) [40, 63], were trained successively by adding bromine atoms, dimers and trimers in the vacuum above them and running machine-learning MD with the recommended settings in VASP for 30 000 steps on each model system using a time step of 2 fs. A Nose–Hoover

thermostat was used to simulate a canonical ensemble at 400 K during machine learning and the application of the FF itself [64]. For these trajectories, the  $c$ -axis was set to 110 Å. Fixed bromine molecules were placed in the vacuum to avoid tentative problems with the machine-learning descriptor, which arise in VASP 6.3 in the case of single bromine atoms without defined local environment.

## Results and discussion

### Bromine adsorption on $h$ -BN/Rh(111)

The adsorption and thermal evolution of bromine on  $h$ -BN was investigated *in situ*. XP spectra of all relevant core levels (N 1s, B 1s and Br 3d) were continuously recorded during background exposure to elemental bromine at a substrate temperature of 170 K and during subsequent heating from 170 to 800 K. To examine the influence on the  $h$ -BN nanomesh, the changes in the N 1s and B 1s core level must be analyzed in detail. Figure 1 provides exemplary fits of the N 1s and B 1s spectra prior to and after low-coverage ( $\leq 0.14$  ML Br) bromine adsorption along with the corresponding quantitative analyses. In addition, we compare the pristine state of  $h$ -BN to the spectrum recorded after TPXPS, i.e. after heating to 800 K. Please refer to the SI for the density and waterfall plots of the complete data set recorded in the N 1s (figure S1) and B 1s (figure S2) regions.

Prior to the adsorption, the N 1s spectrum of  $h$ -BN/Rh(111) shows two signals at 398.80 and 398.14 eV (figure 1(a), top). The peak at higher binding energy (dark blue) corresponds to the pores of the  $h$ -BN nanomesh while the one at lower binding energy (blue) is associated with the wires. The pores and wires of  $h$ -BN differ regarding their interaction with the substrate: while the pores are in close contact to the Rh(111) surface, thus experiencing strong interaction, the wires are hardly influenced by the substrate. Hence, the pores are expected to show an enhanced reactivity towards functionalization compared to the wires. This has already been observed for functionalization with molecular oxygen and atomic hydrogen [42]. Also, the deposition of metal atoms and clusters can be conducted in a spatially confined manner using the nanomesh as a template [65].

Upon adsorption of a rather low bromine coverage of 0.09 ML Br (figure 1(a), bottom), the N 1s spectrum undergoes distinct changes and cannot be described by only two peaks anymore. The pore signal is significantly smaller and shifts to lower binding energies by 0.09 eV. The same shift is observed for the wire signal, which otherwise remains largely unaffected. These uniform shifts of the pore and wire signals are attributed to doping effects [66] and have also been observed in the case of functionalization with hydrogen and oxygen [42]. A new N 1s signal at 398.59 eV (green) replaces the original pore signal, which is also well observable in the quantitative analysis of the N 1s data during the adsorption process (figure 1(b)). Since only the pore signal is significantly influenced by bromine adsorption, we assume that bromine preferentially adsorbs in the pores of the nanomesh.

Consequently, the new signal, gradually replacing the initial pore peak, is attributed to the functionalized pore. This suggests spatial selectivity of the adsorption, which proves the template effect of the  $h$ -BN moiré. Such a behavior has already been observed in similar systems [42, 65, 67].

In the B 1s region, a similar trend is observed. The respective fits and the quantitative analysis are depicted in figures 1(d) and 1(e). Pristine  $h$ -BN/Rh(111) is characterized by two peaks in the B 1s spectrum at 190.33 and 190.75 eV, corresponding to the wires (blue) and pores (dark blue), respectively. Upon adsorption of 0.07 ML Br, the original pore signal decreases and a new peak evolves at 190.65 eV (green), which is attributed to the functionalized pore. In comparison to the N 1s spectrum, the original pore and wire signals undergo only a small shift of 0.02 eV to lower binding energies due to doping. Overall, the B 1s data are perfectly in line with the N 1s spectra and support the assumption of selective functionalization in the pores. Furthermore, we find an additional signal at 191.63 eV (brown), which corresponds to a boron coverage of 0.05 ML. This peak might be the result of a pronounced interaction between boron and molecular bromine, with bromine withdrawing electron density from boron, leading to a shift to higher binding energies. Accordingly, we assume selective bromine adsorption on the boron atoms in the pores of the nanomesh.

Regarding the quantitative analyses, a linear relationship between the intensity of the functionalized pore peak and the bromine exposure would be expected, given that the adhesion coefficient remains unchanged during the adsorption process. This applies, within the margin of error of the fit, quite well for the N 1s as well as B 1s data. Here, it needs to be taken into consideration that unwanted effects such as coverage-dependent photoelectron diffraction might influence the peak intensities to a certain extent.

To investigate the reversibility of the adsorption process, we compare the N 1s and B 1s spectra of the substrate prior to adsorption, i.e. its pristine state, with the spectra of the brominated 2DM recorded after heating to 800 K. Figures 1(c) and (f) provide an overlay of these spectra for the N 1s and the B 1s regions, respectively. In both cases, the pristine state of  $h$ -BN/Rh(111), characterized by a two-peak signature for the pores and wires, is regained after thermal treatment, as is deduced from the perfect agreement of the curves. This indicates that bromine adsorption on the  $h$ -BN nanomesh is fully reversible upon heating.

As a next step, we address the adsorption of different amounts of bromine on  $h$ -BN/Rh(111). In figure 2, waterfall plots of the Br 3d spectra recorded during adsorption and fits of the final spectra are depicted for a low-coverage (0.06 ML Br) and a high-coverage (0.67 ML Br) scenario.

For low coverages (figure 2(a)), a spin-orbit-split Br  $3d_{3/2}$ /Br  $3d_{5/2}$  doublet evolves at 68.51/69.54 eV (green), which is assigned to a single bromine species. From the multiplicity of the spin-orbit-splitting a Br  $3d_{5/2}$ :Br  $3d_{3/2}$  intensity ratio of 3:2 is expected. Accordingly, an intensity ratio of 1.5 was used to fit the doublets, and a peak splitting of 1.03 eV was found. These parameters were kept constant for all doublets. Considering the information obtained from the

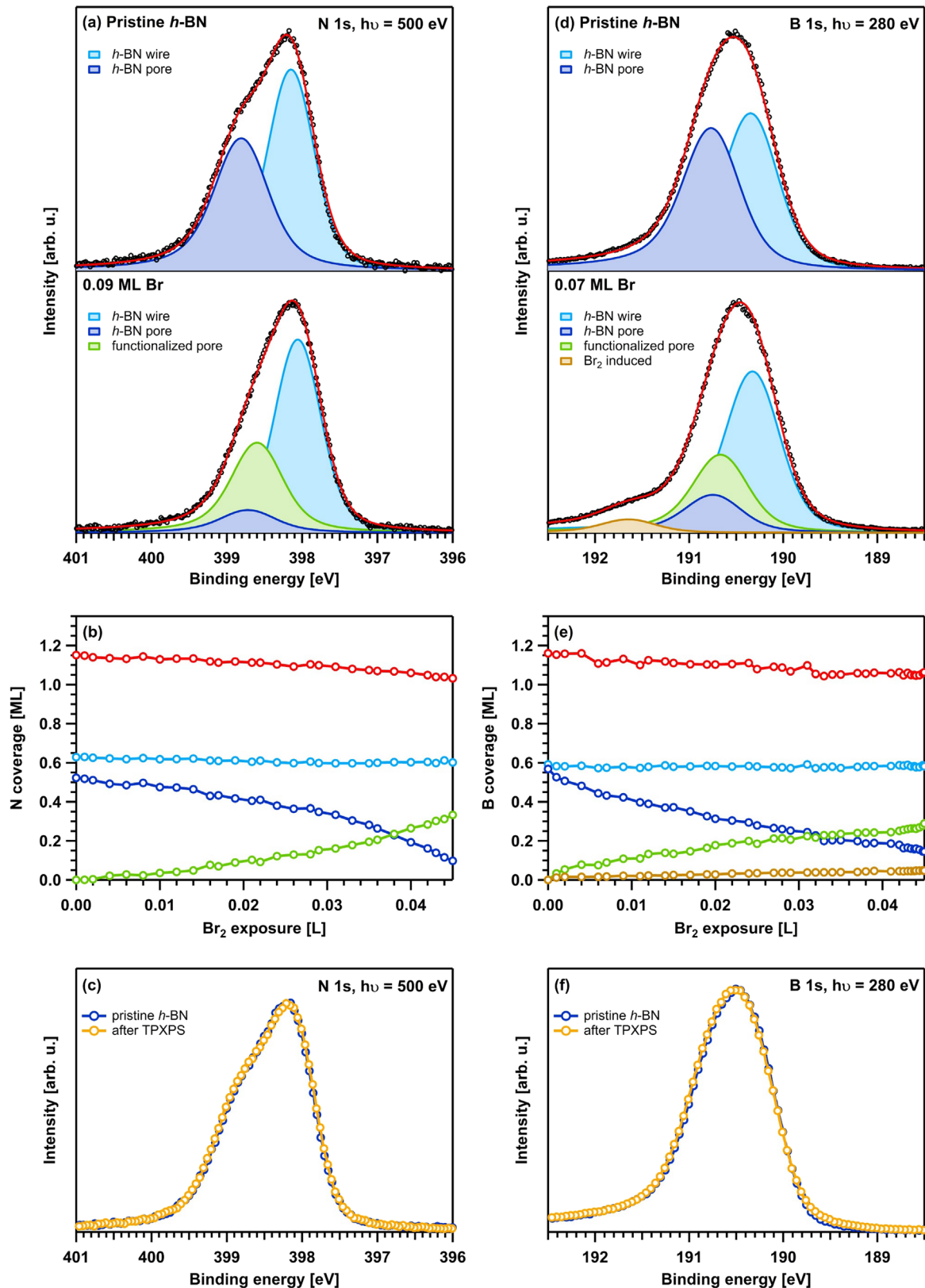


**Figure 1.** (a) Fitted N 1s spectra prior to (top) and after (bottom) bromine adsorption on h-BN/Rh(111) (0.09 ML); (b) quantitative analysis of the N 1s spectra collected during the adsorption; (c) comparison of the N 1s spectrum of pristine h-BN and the spectrum of brominated h-BN after heating to 800 K; (d)–(f) corresponding data for the B 1s region (0.07 ML).

analysis of the N 1s and B 1s region after low-coverage adsorption (see above), the doublet is attributed to molecular bromine selectively adsorbed in the pores of the nanomesh. In

the high-coverage experiment (figure 2(b)), we first observe a shift of the doublet to lower binding energies upon increasing coverage, presumably caused by adsorbate-adsorbate

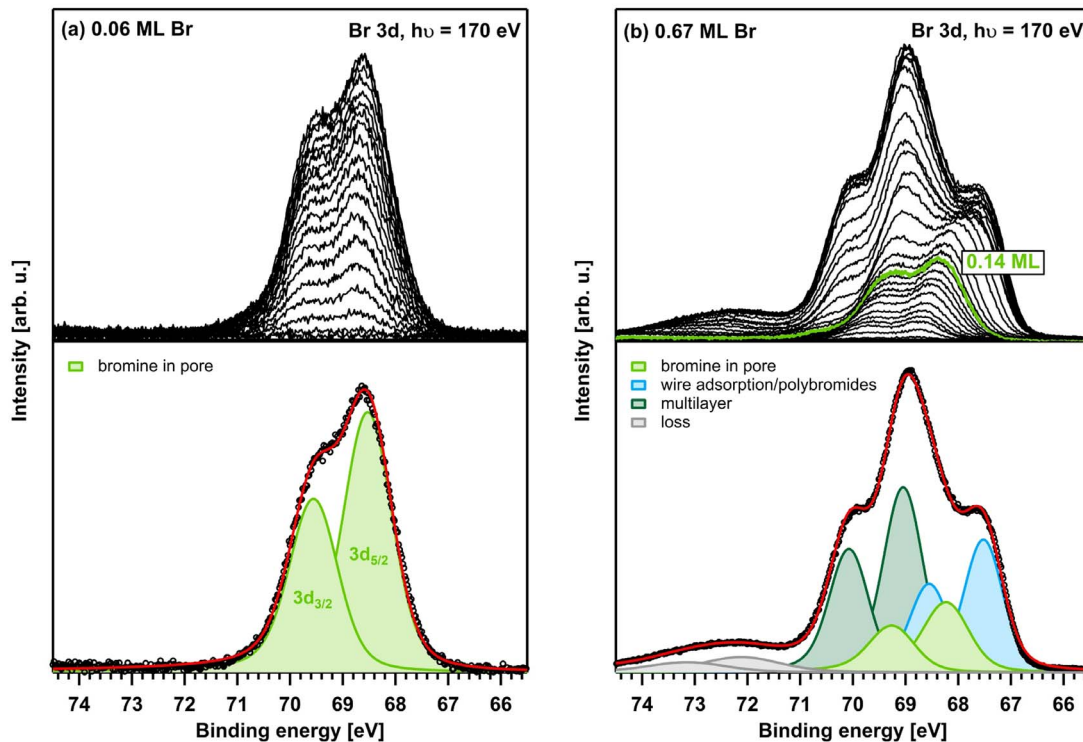


**Figure 2.** (a) Waterfall plot of the Br 3d XP spectra recorded during the low-coverage adsorption (0.06 ML) of elemental bromine on *h*-BN/Rh(111) at 170 K (top) and fit of the final Br 3d spectrum (bottom); (b) corresponding data for the high-coverage adsorption (0.67 ML).

interaction. Further bromine exposure leads to saturation of the doublet assigned to bromine in the pore at a coverage of approximately 0.14 ML Br. Coverages smaller than 0.14 ML, hence, lead to exclusive pore adsorption and reflect very similar situations on the nanomesh. In addition, two new doublets arise. The one at higher binding energies (69.03/70.06 eV; dark green) is assigned to multilayers of molecular bromine in the pores. The one at lower binding energies (67.51/68.54 eV; blue) might belong to bromine adsorbed on the wires of *h*-BN, being less favorable than the adsorption in the pores. Another possible explanation for this doublet is the coverage-dependent formation of polybromides, such as  $\text{Br}_3^-$  or  $\text{Br}_5^-$ , upon increasing pore coverage (see also below). An additional doublet develops at 72.09/73.12 eV (gray), which is attributed to losses during photoemission. Since the intensity ratio of the loss feature and the multilayer signal remains roughly constant, we assign the doublet to a shake-up satellite of the multilayer species.

To study the reactivity and thermal stability of bromine adsorbed in the pores, we conducted a TPXPS experiment in the Br 3d region after the low-coverage bromine adsorption; this coverage guarantees exclusive pore adsorption. The waterfall and density plots in figures 3(a) and (b), respectively, reveal strong changes in binding energy between 170 and  $\sim 240$  K. To gain a deeper understanding of this heating-induced on-surface reaction, we fitted the Br 3d spectra. Fits at selected temperatures are shown in figure 3(c).

At 170 K, the spectrum contains the doublet at 68.54/69.57 eV, typical for molecular bromine adsorbed in the *h*-BN pores (green, see above). Upon heating, this doublet

decreases, and two new doublets evolve at lower binding energies, first at 68.04/69.07 eV (purple) and then another one at 67.76/68.79 eV (magenta). Each doublet corresponds to one new bromine species. We tentatively assign these two new species to polybromides, presumably  $\text{Br}_3^-$  and  $\text{Br}_5^-$ . The existence of polyhalides, such as polybromides and polyiodides, is known from literature [68–70]. The formation of (poly)bromides requires a charge transfer from the substrate, which has already been reported for iodine on graphene [71, 72]. Notably, we find a similar behavior due to beam damage upon intensive x-ray irradiation at 170 K, i.e. new signals evolve at lower binding energies; please refer to the SI (figure S3) for the respective spectra. The binding energies found for the polybromide doublets resemble the binding energies of the additional doublet observed on the low-binding-energy side in the high-coverage experiment (figure 2(b), blue doublet). Hence, it seems likely that this doublet actually indicates polybromide formation upon high bromine dosages. At  $\sim 240$  K, the low-binding-energy doublets assigned to the polybromides decrease and disappear and eventually only one species remains on the surface, characterized by a doublet at 68.55/69.58 eV (orange). This behavior might be explained by decomposition of the polybromides, resulting in a single bromine species in the pores. The binding energy and peak shape of this high-temperature species ( $>240$  K) are indeed very similar (within the experimental uncertainty) to those of the bromine species right after adsorption (170 K). However, a back reaction to molecular bromine is energetically unlikely. Instead, the remaining species might correspond to bromide. We propose the

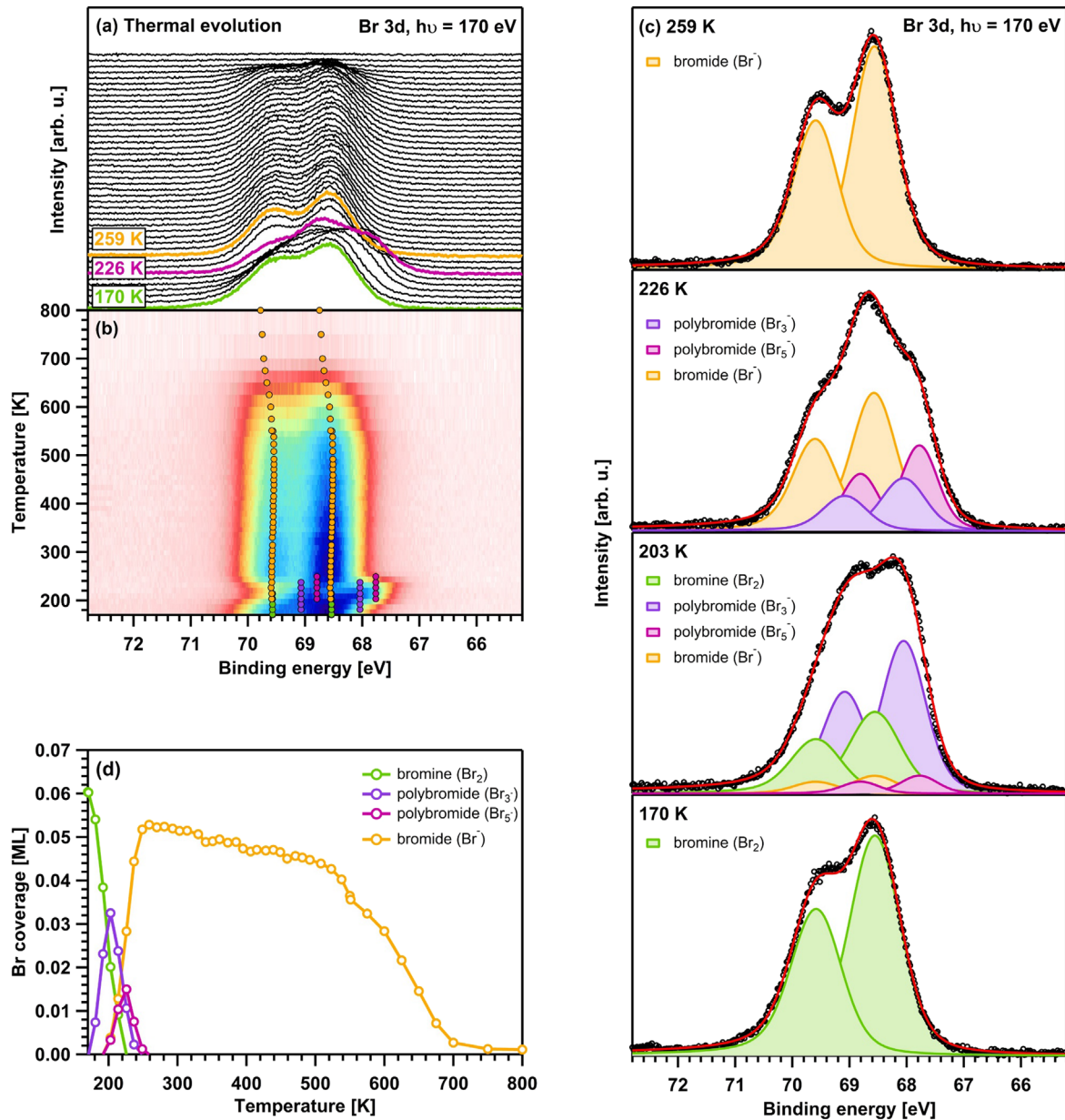


**Figure 3.** (a) Waterfall and (b) density plot of the Br 3d spectra recorded during the TPXPS experiment (170–800 K); (c) fits at selected temperatures; (d) quantitative analysis of the TPXPS data.

following reaction pathway to explain our observations: thermal activation leads to the evolution of bromide, which immediately reacts with the excess of bromine molecules to form polybromides. At temperatures above 240 K, molecular bromine has been completely converted to bromide, and the polybromides decompose to form bromide on the surface. The waterfall and the density plot suggest a high thermal stability of the bromide adsorbed in the pores. The decomposition temperature of the polybromides and the desorption temperature of bromide can be derived more accurately from the quantitative analysis of the TPXPS data (figure 3(d)): decomposition of the polybromides occurs at  $\sim 240$  K, and at higher temperatures only bromide resides in the pores, which desorbs at  $\sim 640$  K. This high thermal stability indicates strong/covalent bonding to *h*-BN.

To exclude the intercalation of bromine upon adsorption at 170 K, we analyzed the signals in the Rh 3d region. The respective spectra are shown in the SI (figure S4). Prior to *h*-BN growth, two Rh 3d signals are observed, corresponding to the bulk and the surface atoms (surface core level shift) of Rh(111). For *h*-BN/Rh(111), the surface component is lowered but still visible. This behavior can be explained by the weak interaction between the *h*-BN wire region and the substrate, which causes part of the substrate to behave like the bare Rh(111) surface. Upon bromine adsorption at 170 K, only an overall damping of both the Rh 3d bulk and surface contributions is observed. In particular, the Rh 3d surface component does not reveal a distinct shift to higher binding energies, which would be expected in the case of a direct interaction with bromine. Therefore, we propose that no

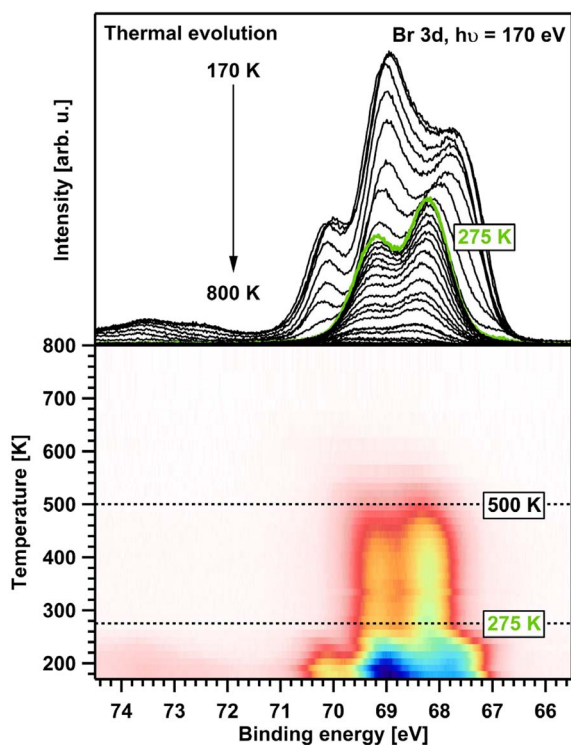


**Figure 4.** Waterfall (top) and density (bottom) plot of the Br 3d XP spectra recorded during heating of 0.27 ML of bromine on *h*-BN/Rh(111) from 170 to 800 K.

intercalation occurs upon bromine adsorption. Additional proof is provided by a detailed study on the adsorption and thermal stability of bromine on clean Rh(111) [73], which reveals that the desorption temperature for bromine on Rh(111) ( $\sim 1000$  K) is much higher than the value of 640 K observed for bromine on *h*-BN/Rh(111). This indicates that heating also does not lead to intercalation.

A TPXPS experiment was also performed with a high bromine coverage (0.27 ML Br). The corresponding Br 3d waterfall and density plots are provided in figure 4.

The doublets assigned to the bromine multilayers and to adsorption on the wires of the nanomesh (or polybromides) start to decrease due to desorption directly upon heating, suggesting a weak bonding/low stability of these species. Above 275 K, only one doublet remains, which is attributed to bromide in the pores since its binding energies are seemingly identical with the high-temperature species found for the low-coverage adsorption. Notably, in this case, bromide desorbs at a significantly lower temperature ( $\sim 500$  K versus  $\sim 640$  K). We suggest an associative desorption mechanism of bromine. However, the observed decrease regarding the desorption temperature cannot only be explained by a second order desorption process. Additionally, we tentatively assume that the higher desorption temperature at low coverages could be explained by diffusion limitation of the desorption of bromine. The higher pore coverage facilitates the association of two bromides to one bromine molecule next to each other and thus no diffusion is required. A similar behavior has been

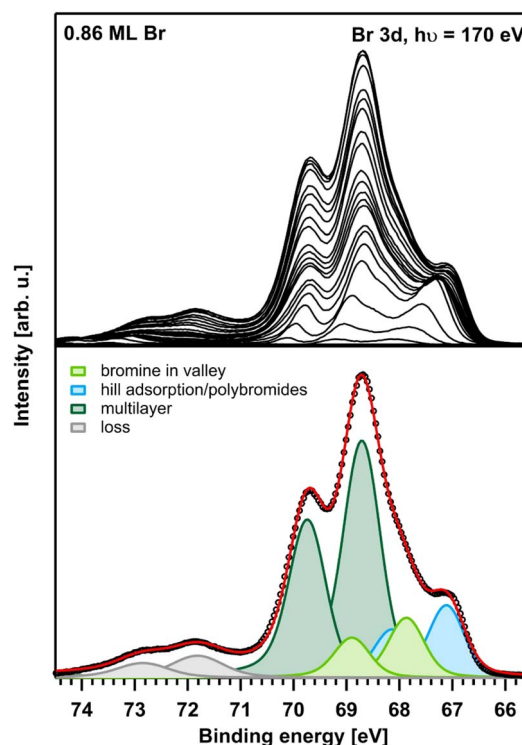


**Figure 5.** Waterfall plot of the Br 3d XP spectra recorded during adsorption of elemental bromine (0.86 ML) on graphene/Rh(111) at 170 K (top) and fit of the final Br 3d spectrum (bottom).

observed for hydrogen desorption from graphene on Ni(111) [16].

### Bromine adsorption on graphene/Rh(111)

After successful selective bromine functionalization of the *h*-BN nanomesh on Rh(111), we studied bromine adsorption on Rh(111)-supported graphene. Graphene/Rh(111) also exhibits a moiré pattern with stronger bonded regions close to the substrate ('valleys') and weaker bonded, elevated regions ('hills'). This buckling is, however, less pronounced than for *h*-BN/Rh(111). Elemental bromine was again dosed via background exposure onto the substrate at 170 K. The waterfall plot of the Br 3d spectra, visualizing the adsorption process *in situ*, and the fit of the final spectrum (0.86 ML Br) are depicted in figure 5.

Here, interpretation of the spectra is not as intuitive as in the case of bromine adsorbed on *h*-BN. From low coverages on, a rather complex spectral shape arises, presumably consisting of several overlapping peaks. The almost simultaneous growth of several species indicates that for bromine adsorption on graphene/Rh(111) no preferred adsorption site exists. Hence, we conclude that no spatially selective bromine functionalization occurs. Fitting the final Br 3d spectrum requires four doublets, which are assigned in analogy to the spectra recorded for the high-coverage adsorption of bromine on *h*-BN/Rh(111): bromine adsorbed in the valleys (67.86/68.89 eV; green), bromine adsorbed on the hills or



polybromides (67.09/68.12 eV; blue), multilayer formation (68.69/69.72 eV; dark green) and loss features (71.80/72.83 eV; gray). TPXPS was employed to study the thermal stability in the temperature range from 170 to 800 K. Please refer to the SI for the respective waterfall and density plots (figure S5(a)). Bromine adsorbed in multilayers desorbs already below room temperature. Between  $\sim 300$  and 400 K, several overlapping Br 3d doublets are observed, probably belonging to bromine adsorbed on the hills and valleys. Above 400 K, only small amounts of bromine remain on the surface. Even at very high temperatures of 800 K, we still observe a residual Br 3d doublet at 68.74/69.77 eV (0.007 ML Br). Due to its high thermal stability, we assume that minor amounts of bromine intercalate underneath the graphene layer upon heating.

To obtain an insight into the influence of bromine adsorption on graphene/Rh(111), C 1s spectra were recorded prior to adsorption, after adsorption and after heating to 800 K; figure 6 provides the corresponding fits. The full set of C 1s spectra acquired during heating from 170 to 800 K are shown in the SI (figure S5(b)). The pristine graphene spectrum (figure 6(a)) displays two peaks at 285.23 and 284.65 eV that belong to the valleys (dark blue) and hills (blue) of the moiré, respectively. An additional peak at 284.12 eV arises due to defects of the graphene layer and is associated with  $sp^3$ -hybridized carbon, i.e. carbide (light blue) [74]. Upon bromine adsorption (figure 6(b)), the signal intensity of all three peaks is dampened and we observe a shift to lower binding energies by 0.13, 0.18 and 0.29 eV for the valley, hill and defect components, respectively. This shift can be explained by doping effects caused by the interaction of bromine with graphene [66, 72]. However, no significant changes regarding the peak shapes are observed, supporting the assumption that no spatially defined bromine adsorption takes place. Moreover, an additional peak develops at a higher binding energy of 286.20 eV (brown). It corresponds to 0.14 ML carbon and is assigned to graphene interacting with bromine molecules. Upon heating to room temperature (figure S5 in the SI), most of the bromine desorbs, and in the C 1s spectra the signal dampening and the shifts to lower binding energies caused by doping effects are reversed. Also, the signal at 286.20 eV indicating the interaction between molecular bromine and graphene disappears. This behavior shows that the residual bromine species observed above room temperature have a negligible influence on the 2DM. Figure 6(c) provides the fitted C 1s spectrum recorded after the TPXPS experiment, i.e. after heating to 800 K. Here, the pristine state of the graphene layer is regained. Hence, bromine adsorption on graphene/Rh(111) seems to be an almost fully reversible process except for the small amount of intercalated bromine.

## Theoretical results

To complement the experimental findings, a theoretical study on the adsorption of bromine on Rh(111)-supported *h*-BN and graphene was performed. Figure 7 shows the optimized

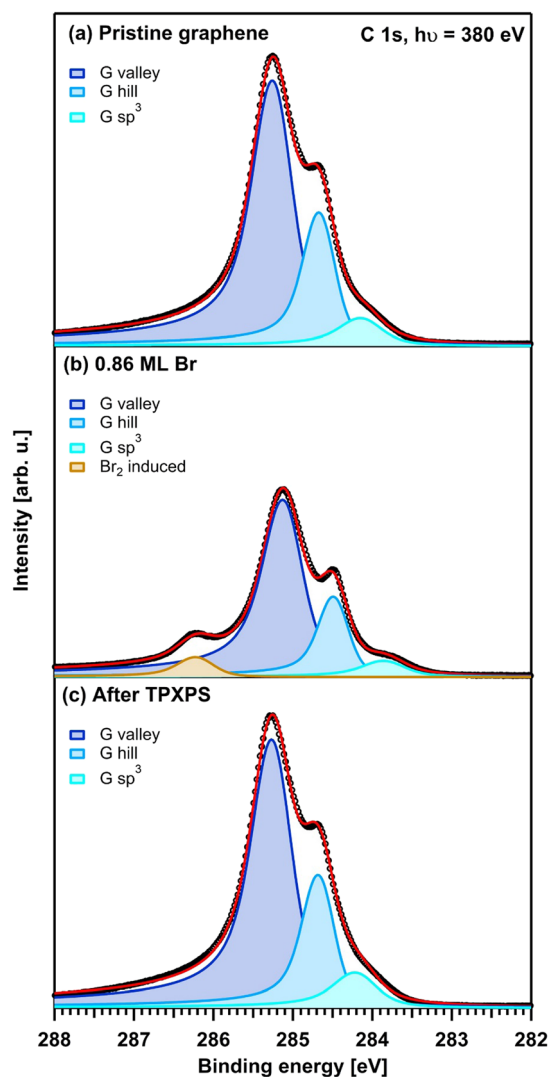


**Figure 6.** Fitted C 1s XP spectra recorded prior to adsorption (top), after adsorption of 0.86 ML Br (center) and after the TPXPS experiment, i.e. heating from 170 to 800 K (bottom).

structures of Rh(111)-supported *h*-BN and graphene. A three-layer model was chosen as the substrate and proved to be sufficient (figure S6 in the SI).

In the pore/valley region, both systems have similar spacing between the topmost Rh(111) atom layer and the *h*-BN/graphene lattice, that is 2.10 Å between B/N and Rh, and 2.05 Å between C and Rh. In the wire/hill region, on the other hand, the maximum distance to the substrate differs significantly for the two systems. For the *h*-BN system, a much larger maximum distance (4.44 Å) is found than in the graphene system (3.58 Å). The stronger buckling of *h*-BN/Rh(111) presumably leads to a more pronounced difference regarding the chemical reactivity of the pores and wires, thereby causing selectivity for adsorption of adatoms. The electronic properties of both systems are illustrated by charge density difference plots and simulated STM images, in which we clearly observe that the interaction between *h*-BN/graphene and the metal substrate is mainly restricted to the pore/

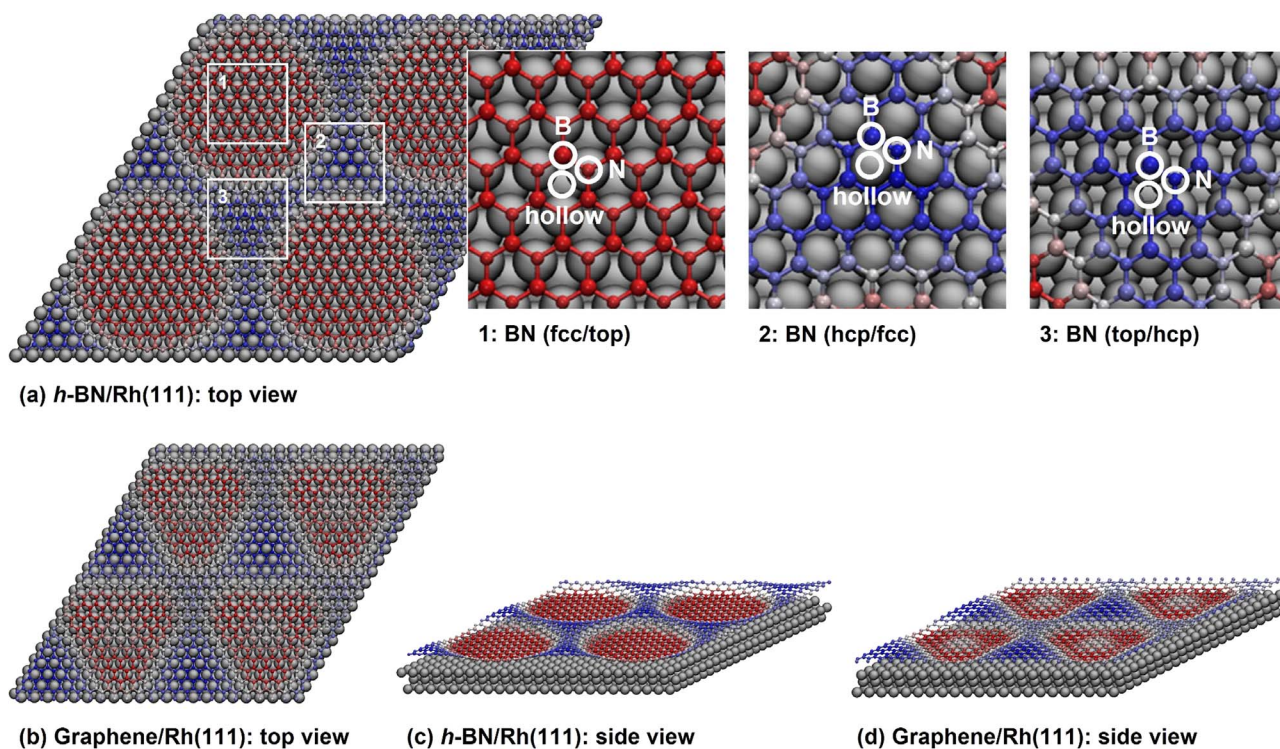


**Figure 7.** (a) Top view of four unit cells of the *h*-BN/Rh(111) nanomesh. The three characteristic regions BN (fcc/top), BN (hcp/fcc) and BN (top/hcp) are marked. Larger cutouts of these regions visualize the 9 possible adsorption sites for bromine; (b) top view of four unit cells of the graphene/Rh(111) moiré; (c) and (d) corresponding side views of *h*-BN and graphene on Rh(111). The pore and wire regions are colored red and blue, respectively.

valley region. See SI for the respective data (figures S7 and S8).

Figure 7(a) also illustrates the different surface regions and adsorption sites that we will refer to in the following. In the case of *h*-BN/Rh(111), we differentiate three characteristic regions: BN (fcc/top) in the pores, and BN (hcp/fcc) and BN (top/hcp) on the wires. If we only consider highly symmetrical positions, an adsorbate could bind to a nitrogen atom, to a boron atom or in the center of the six-membered ring (hollow) in each of the above-mentioned three different regions. This leads to 9 possible adsorptions sites. Analog bonding configurations apply for graphene/Rh(111).

To support the experimental results regarding bromine adsorption on Rh(111)-supported *h*-BN and graphene, binding energies of bromine molecules and atoms on the 2DM were calculated. For the *h*-BN nanomesh, it is expected that adsorption in the pores is preferred. Thus, this is a first test if the theoretical model agrees with the experimental findings. For adsorbed molecular bromine, the calculated adsorption energies for the three different regions of the nanomesh/moiré structure are shown in table 1, along with the Br–Br bond lengths in the respective optimized geometries.

We observe that the bromine molecules preferentially bind to the boron atoms in the pores of *h*-BN (figure 8(a)), which fits the experimental results. Regarding the bond lengths, significant elongation is observed for the bromine molecules in the pores, indicating strong binding to the surface. For graphene, the bonding energy to the valley is much weaker. The bond length, however, is still significantly

**Table 1.** Relative energies and bond lengths of molecular bromine adsorbed on Rh(111)-supported *h*-BN and graphene.

Region	h-BN/Rh(111)		Graphene/Rh(111)	
	<i>E</i> [eV]	Br–Br bond length [Å]	<i>E</i> [eV]	Br–Br bond length [Å]
(fcc/top)	−2.0	3.5	−1.2	3.8
(hcp/fcc)	−0.18	2.4	−0.55	2.4
(top/hcp)	−0.19	2.4	−0.59	2.5
vacuum	0.00	2.3	0.00	2.3

elongated. These findings are supported by 2D charge density distributions (figures S9 and S10), which even imply that the bromine molecule is essentially split into two bromine atoms. However, we cannot unambiguously determine if the Br–Br bond is actually broken or only elongated.

To test the energetics of the adsorption of bromine atoms, the geometries of the 9 possible adsorption sites were optimized, whereby only the *z*-coordinate of the adsorbed bromine atom was allowed to change together with the nearest atoms on the nanomesh, thus restricting them to the respective site. The relative energies were calculated by taking the absolute energies of two unit cells with adsorbates and subtracting the energies of one bromine molecule in vacuum and two clean *h*-BN/graphene unit cells as reference. For graphene/Rh(111), the same adsorption sites were chosen. The two positions on top of the carbon atoms only differ regarding

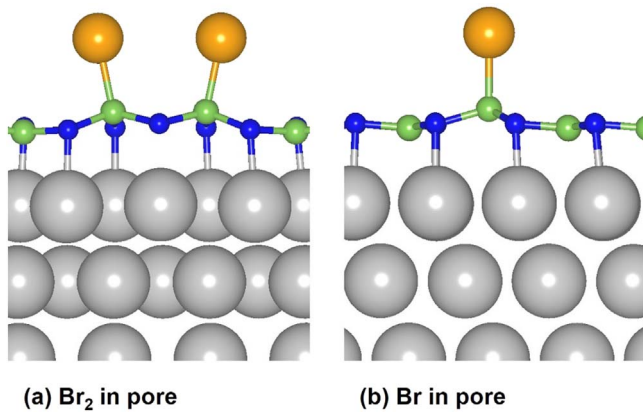


**Figure 8.** Vertical cut-through of the optimized structures of (a) bromine molecules and (b) bromine atoms adsorbed in the pores of the *h*-BN/Rh(111) nanomesh. Boron, nitrogen, bromine and rhodium atoms are colored green, blue, orange and gray, respectively.

**Table 2.** Relative energies of 2 bromine atoms adsorbed on Rh(111)-supported *h*-BN and graphene, referenced to bromine molecules in vacuum.

<i>h</i> -BN/Rh(111)		Graphene/Rh(111)	
adsorption site	<i>E</i> [eV]	adsorption site	<i>E</i> [eV]
(fcc/top), B	−2.0	(fcc/top), C <sub>1</sub>	−1.6
(fcc/top), N	−0.58	(fcc/top), C <sub>2</sub>	−1.8
(fcc/top), hollow	−0.62	(fcc/top), hollow	−1.6
(hcp/fcc), B	1.2	(hcp/fcc), C <sub>1</sub>	−0.21
(hcp/fcc), N	1.4	(hcp/fcc), C <sub>2</sub>	−0.23
(hcp/fcc), hollow	1.3	(hcp/fcc), hollow	−0.19
(top/hcp), B	1.3	(top/hcp), C <sub>1</sub>	−0.51
(top/hcp), N	1.4	(top/hcp), C <sub>2</sub>	−0.65
(top/hcp), hollow	1.4	(top/hcp), hollow	−0.54
vacuum	0.00	vacuum	0.00

the metal atom configuration beneath them: C<sub>1</sub> (hollow) and C<sub>2</sub> (top). The resulting relative energies for both systems are listed in table 2.

For the adsorption of bromine atoms on *h*-BN/Rh(111), the energetically by far most favorable adsorption site is the boron atom in the pore (fcc/top). This bonding situation is visualized in figure 8(b), in which the boron atoms even seem to be pulled out of the nanomesh by the strong bonding to bromine. The other two possible positions in the pore are also preferred over the wire regions (hcp/fcc and top/hcp), which even reveal positive adsorption energies, showing that wire adsorption is thermodynamically unfavorable. This supports the experimental findings that propose selective bromine adsorption on boron atoms in the pores of the nanomesh. Only for high bromine coverages, weak physisorption on the wires seems to take place (figure 2(b), blue doublet). Instead of wire adsorption, it is also possible that the additional low-binding-energy doublet observed during high-coverage adsorption is caused by polybromide formation. The adsorption energies of bromine atoms on boron in the pore and of bromine molecules in the pore, also binding on boron

atoms, are identical (−2.0 eV; compare tables 2 and 1). This indicates that the bromine molecules indeed almost completely dissociate upon adsorption in the pore. For graphene, the C<sub>2</sub> site in the valley (fcc/top) is the most favorable binding site for bromine atoms (−1.8 eV). The C<sub>1</sub> and the hollow sites are, however, only slightly higher in energy (by ~0.20 eV). Adsorption on the hills (hcp/fcc and top/hcp) is significantly higher in energy (by ~1.0 eV). Nonetheless, the respective adsorption energies are still negative, which implies that adsorption on the hills of the graphene moiré is thermodynamically stable. In comparison to the *h*-BN nanomesh, the energetic difference between the valley and the hill regions of the graphene moiré is less pronounced, which might explain why no clear spatial selectivity of the bromine functionalization is observed in the experiment. In the SI, corresponding charge density distributions and optimized structural models are provided (figures S9 and S10).

To examine the electronic interaction of bromine atoms/molecules with Rh(111)-supported *h*-BN and graphene, we calculated core level shifts (CLS, figure S11), partial charges (tables S2 and S3) and the density of states (figure S12). The respective data and a brief discussion are provided in the SI. The calculated CLS support qualitatively the observed shift of bromine in the pores/valleys to higher binding energies compared to bromine adsorbed on the wires/hills. The Bader charge analysis reveals that all bromine species on Rh(111)-supported *h*-BN and graphene are negatively charged, i.e. that bromine acts as an electron acceptor. The assumed charge transfer from the substrate seems thus to be confirmed. In addition, the pore region of the *h*-BN nanomesh is also polarized with the nitrogen atoms being negatively (−2e) and the boron atoms being positively (+2e) charged. This polarization presumably promotes the interaction between bromine and boron, leading to boron as the preferred adsorption site. The distinct binding of bromine to boron might be crucial for the spatial selectivity of bromine adsorption on the *h*-BN/Rh(111) nanomesh, which cannot be observed for the graphene moiré.

In the following, bromine adsorption on *h*-BN/Rh(111) is investigated in even more detail. To gain deeper insights into the adsorption of bromine in the pores of the *h*-BN nanomesh, the geometries of 2–20 bromine molecules in the pore were optimized. Selected optimized geometries are shown in figure 9. Please note that no global optimizations of these structures were done. Instead, several local minima were optimized for 2–5 bromine molecules. For larger numbers, the molecules were placed referring to the findings for 2–5 molecules and taking reasonable guesses regarding symmetry and size into consideration. Due to the large size of the systems and the ‘soft’ character of the bromine molecules, it was difficult to converge the geometry optimizations with VASPs internal geometry optimization routines. Instead of reaching the usual gradient convergence criterion (0.03 eV Å<sup>−1</sup>), the total energy criterion was used to indicate convergence. Convergence was reached if the change in total energy dropped below 1 × 10<sup>−5</sup> eV between two geometry optimization steps, which should be quite accurate considering the large size of the system and the large absolute energy.

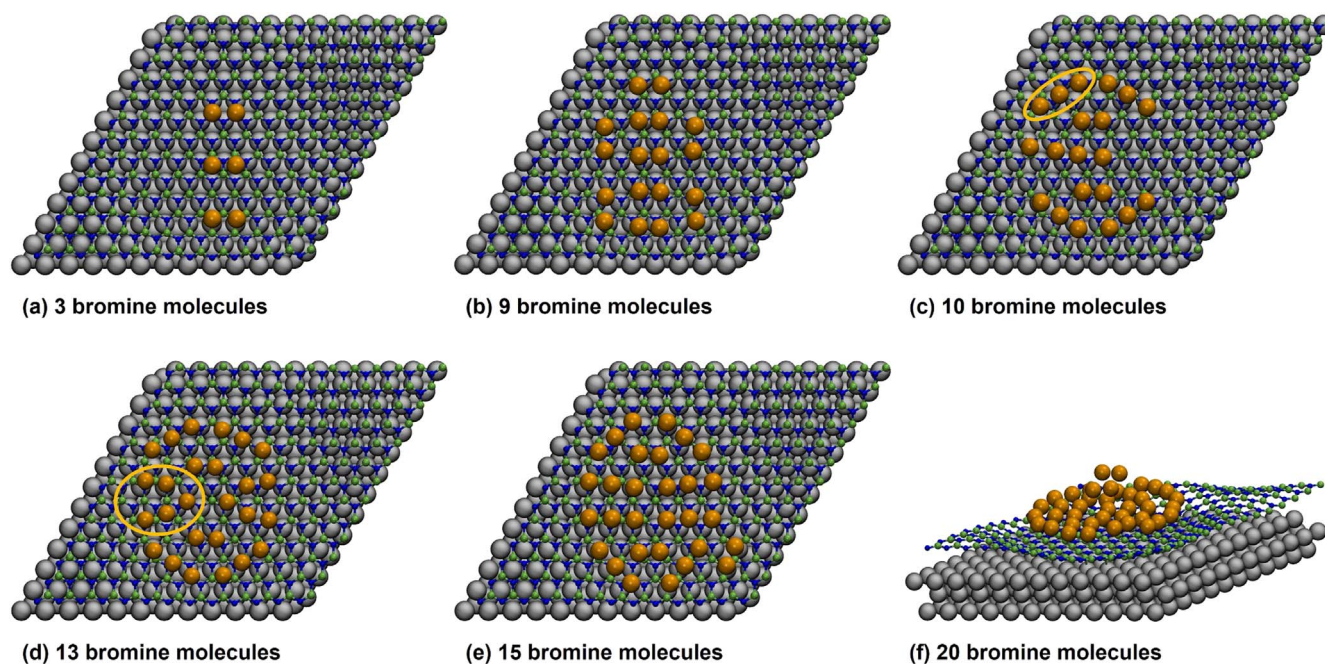


**Figure 9.** Optimized structures for different numbers of bromine molecules within the pore region of the *h*-BN/Rh(111) nanomesh. Boron, nitrogen, bromine and rhodium atoms are colored green, blue, orange and gray, respectively. Polybromides are marked by yellow circles.

Up to 9 molecules in the pore (0.13 ML), isolated and well-distinguishable bromine molecules are observed (figure 9(b)). For larger bromine coverages, polybromides ( $\text{Br}_3^-$  and  $\text{Br}_5^-$ ) seem to be formed (figures 9(c) and (d)). Additionally, figure S13 in the SI provides corresponding simulated STM images that also show increasing interaction of the bromine molecules upon increasing pore coverage. This suggests that polybromide formation is a rather likely process to occur in the pores, hence supporting our assumption that polybromides are formed for high coverages and upon mild heating. The maximum pore coverage is reached for 13–14 bromine molecules (0.18–0.19 ML). Even higher coverages lead to adsorption on the rim positions (figure 9(e)) and eventually to multilayer formation (figure 9(f)). This is in quite good agreement with the value derived from the high-coverage adsorption experiment that suggests pore saturation for a coverage of approximately 0.14 ML (figure 2(b)).

Furthermore, the desorption energetics of bromine on *h*-BN/Rh(111) were studied. Four different processes were addressed: desorption of a bromine molecule adsorbed in the empty pore, desorption of a bromine molecule adsorbed on the empty wire (BN (top/hcp)), desorption of a bromine molecule adsorbed in the filled pore (13 molecules in the pore) and desorption of a molecule adsorbed in the multilayer (19 molecules in the pore). The resulting energy diagrams are shown in figure S14 in the SI. The energetic barrier for desorption from the pore is comparably high ( $\sim 2.1$  eV), which is a sign of strong bonding to the nanomesh. Desorption from the wire position, on the other hand, reveals a very small energetic barrier of  $\sim 0.2$  eV. This indicates that bromine adsorption on the wires is likely to be unstable. Both desorption energies agree well with the results of the adsorption geometry optimizations in table 1. Desorption from the full

pore requires significantly less energy ( $\sim 0.6$  eV) than in the case of the empty pore, which might be attributed to diffusion limitation at low pore coverages. A very small desorption barrier of  $\sim 0.2$  eV proves bonding of bromine to the second layer to be very weak. The energetical values were determined using the PBE functional in combination with the VASP PAW approach, which delivered good results in similar studies in literature [75, 76]. Nevertheless, it is not the most sophisticated level of theory, and thus errors of approximately  $\pm 0.2$  eV need to be taken into consideration. However, from the trend deduced from the desorption energetics it can be expected that multilayer and wire desorption occur already at rather low temperatures while bromine adsorbed within a monolayer in the pore is thermally relatively stable. Additionally, a decreasing desorption temperature for an increasing pore coverage should be observed. The experimental data obtained in the TPXPS measurements are in good agreement with these predictions.

Finally, we wanted to explore the interaction of the adsorbed bromine species on the *h*-BN nanomesh on longer timescales. To this end, a VASP machine-learning FF for this system was parametrized. Usually, the system of interest would be simulated by means of *ab initio* molecular dynamics (AIMD), during which the FF is learned on the fly and replaces the DFT description gradually such that a considerable amount of coordinate space can be sampled, and data can be included into the machine-learning FF. This was, however, not possible due to the large size of the investigated system. Hence, an alternative approach was used: model systems of the three different regions of the nanomesh, BN(fcc/top), BN(hcp/fcc) and BN(top/hcp), were learned successively at 400 K. Figure S15 in the SI shows the optimized cutouts used. After the learning process converged (no AIMD steps during

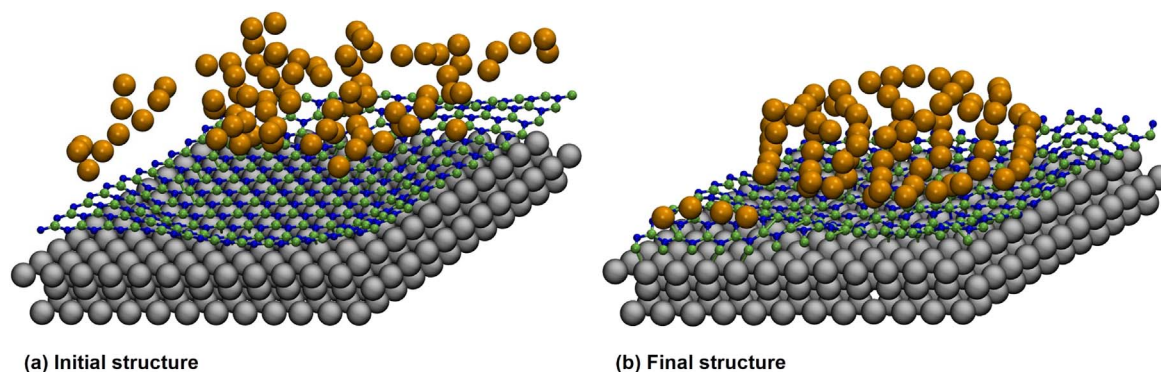


**Figure 10.** Simulation starting from an empty *h*-BN pore with 40 bromine molecules 10 Å above the surface: (a) initial and (b) final structure. Boron, nitrogen, bromine and rhodium atoms are colored green, blue, orange and gray, respectively.

many thousands of time steps), the resulting machine-learning FF was used to run MD of a whole nanomesh cell with bromine on it, which was impossible with AIMD before. Using this advanced machine-learning FF, the adsorption behavior of bromine molecules on the *h*-BN/Rh(111) nanomesh can be simulated. 10 MD trajectories (50 ps each) with a 2 fs time step were simulated as a first benchmark at 400 K. The machine-learning FF, although never learned on the full moiré structure, was able to hold the pattern stable, which shows that it is indeed sufficient to describe the whole system at least qualitatively correct. Thereafter, bromine adsorption on the nanomesh was simulated, starting from an empty pore with 40 bromine molecules placed 10 Å above the surface. The starting structure (bromine gas above the *h*-BN nanomesh) and the final frame of one calculated MD trajectory (out of 20) for this process are shown in figure 10.

All bromine molecules seem to adsorb in the pore region, whereby a multilayer is formed after saturation of the pore. For a quantitative analysis of the dynamics, three parameters were looked at: radial distribution functions (RDF) of bromine with itself, boron and nitrogen (figure S16(a)), a 2D-averaged spatial distribution of bromine along the surface (figure S16(b)) and the time-dependent surface coverage (figure S16(c)). The latter was calculated by looping through all bromine atoms in the system in each time frame and assigning one atom as bonded to the surface if the distance to an arbitrary B or N atom in the system is lower than 3.5 Å, thereby neglecting the second adsorption layer. The RDF analysis shows that the B–Br bond is shorter than the Br–Br bond (2.1 versus 2.3/2.7 Å), indicating a pronounced interaction between bromine and boron. The two-peak structure arising in the Br–Br distribution might be caused by the different Br–Br distances regarding the first and the second layer. The longer bonds can be assigned to the bromine in close contact to the nanomesh while the bromine molecules in the multilayer, being similar to free bromine molecules, exhibit shorter bonds. In the corresponding two-dimensional bromine atom density plot, sharp spots are exclusively located on top of the boron atoms in the pores. Outside the pore, the probability of finding a bromine atom is almost zero. In addition, some background noise can be observed, probably originating from the weakly bound multilayer, which seems

to be much more thermally mobile than the first layer. The time-dependent surface coverage reveals a gradually slowing adsorption process, converging at about 0.30 ML (22 bromine molecules).

## Conclusion

In this study, the adsorption, reactivity and thermal stability of bromine on Rh(111)-supported *h*-BN and graphene were investigated. To gain a detailed understanding of these systems on the molecular level, we used high-resolution XPS and TPXPS to follow the respective processes *in situ*. For the adsorption of low coverages of bromine on the *h*-BN nanomesh at 170 K, we find that molecular bromine adsorbs exclusively in the pores, with boron being the preferred adsorption site. This demonstrates selective functionalization of the 2DM and confirms the template effect of the nanomesh. Upon heating, polybromides are formed, which decompose at about 240 K to form bromide in the pores. This species is quite stable and remains on the surface up to ~640 K. Due to this high thermal stability, we assume strong/covalent bonding of bromide to *h*-BN. Interestingly, the desorption temperature of bromide decreases upon increasing pore coverage, which suggests that diffusion limitation plays a role at low coverages. After heating to 800 K, pristine *h*-BN/Rh(111) is regained, indicating full reversibility of the functionalization. For bromine adsorption on graphene/Rh(111) at 170 K, we do not observe spatial selectivity in the Br 3d and C 1s spectra. In the C 1s spectra, we nevertheless find clear indication of interaction between graphene and bromine. Bromine exhibits a comparably low thermal stability on Rh(111)-supported graphene; most of the bromine desorbs already below room temperature. At higher temperatures, a small amount of bromine intercalates underneath the graphene layer. Apart from this, bromine adsorption on the graphene moiré is reversible upon heating to 800 K.

The experimental findings were supported by a comprehensive theoretical study, in which DFT was used to explore the structure and substrate interaction of Rh(111)-supported *h*-BN and graphene as well as the characteristics of bromine adsorption on the 2DM. For the first time, MD using

a machine-learning FF were employed to simulate bromine adsorption on the *h*-BN nanomesh. In the case of the *h*-BN nanomesh, we find a stronger buckling than for the graphene moiré, causing a more pronounced difference in reactivity between pores and wires. Furthermore, adsorption energies of molecular and atomic bromine were determined, suggesting the pores/valleys to be favorable for adsorption. This preference is strongest for the boron atoms in the pores of the nanomesh. The substantial corrugation of the nanomesh and the preferable interaction of bromine with boron are likely the reasons for the observed spatial selectivity of the functionalization. Regarding the *h*-BN nanomesh, DFT supports the possibility of polybromide formation. Moreover, the MD simulation of bromine adsorption on the *h*-BN nanomesh also confirms its pore selectivity.

## Outlook

Our study has proven that the synergistic combination of XPS and theoretical calculations is a very powerful tool for the investigation of the chemical reactivity of Rh(111)-supported *h*-BN and graphene towards bromine. Both, generally rather inert 2DM are observed to interact with bromine. In the case of the *h*-BN/Rh(111) nanomesh, we were able to demonstrate selective covalent functionalization. Such distinct chemical modification is a promising route to design 2DM with desirable properties, which is crucial for their applicability in real-world devices.

To obtain a more detailed insight into the structural identity of the supported 2DM and its changes upon covalent functionalization, further studies employing microscopic techniques, such as scanning tunneling microscopy (STM), transmission electron microscopy (TEM) or atomic force microscopy (AFM), should be conducted. Also, a thorough analysis of the electronic properties of the pristine and functionalized 2DM, e.g. via the means of scanning tunneling spectroscopy (STS) or angle-resolved photoemission spectroscopy (ARPES), would be recommendable for future works.

## Acknowledgments

Measurements were carried out at the BESSY II electron storage ring operated by the Helmholtz-Zentrum Berlin (HZB) für Materialien und Energie. We would like to thank HZB for the allocation of beamtime and the BESSY II staff for support during the beamtime. This work was funded by the DFG within SFB 953 ‘Synthetic Carbon Allotropes’, project no. 128849149, and SFB 1452 ‘Catalysis at Liquid Interfaces’, project No. 431791331. EMF and CP thank the Fonds der Chemischen Industrie for financial support. The authors gratefully acknowledge the scientific support and HPC resources provided by the Erlangen National High Performance Computing Center (NHR@FAU) of the Friedrich-Alexander-Universität Erlangen-Nürnberg (FAU) under the NHR project b146dc. NHR funding is provided by federal

and Bavarian state authorities. NHR@FAU hardware is partially funded by the German Research Foundation (DFG) – 440719683.


## Data availability statement

All data that support the findings of this study are included within the article (and any supplementary files).

## ORCID iDs

Eva Marie Freiberger  <https://orcid.org/0000-0001-7593-4308>

Julien Steffen  <https://orcid.org/0000-0001-7933-9557>

Natalie J Waleska-Wellenhofer  <https://orcid.org/0000-0002-5212-0368>

Felix Hemauer  <https://orcid.org/0000-0003-1226-0056>

Valentin Schwaab  <https://orcid.org/0000-0002-5441-8846>

Andreas Görling  <https://orcid.org/0000-0002-1831-3318>

Hans-Peter Steinrück  <https://orcid.org/0000-0003-1347-8962>

Christian Papp  <https://orcid.org/0000-0002-1733-4387>

## References

- [1] Novoselov K S, Geim A K, Morozov S V, Jiang D, Zhang Y, Dubonos S V, Grigorieva I V and Firsov A A 2004 Electric field effect in atomically thin carbon films *Science* **306** 666–9
- [2] Lalmi B, Oughaddou H, Enriquez H, Kara A, Vizzini S, Ealet B and Aufray B 2010 Epitaxial growth of a silicene sheet *Appl. Phys. Lett.* **97** 223109
- [3] Dávila M E, Xian L, Cahangirov S, Rubio A and Le Lay G 2014 Germanene: a novel two-dimensional germanium allotrope akin to graphene and silicene *New J. Phys.* **16** 095002
- [4] Li L, Yu Y, Ye G J, Ge Q, Ou X, Wu H, Feng D, Chen X H and Zhang Y 2014 Black phosphorus field-effect transistors *Nat. Nanotechnol.* **9** 372–7
- [5] Mannix A J *et al* 2015 Synthesis of borophenes: anisotropic, two-dimensional boron polymorphs *Science* **350** 1513–6
- [6] Corso M, Auwärter W, Muntwiler M, Tamai A, Greber T and Osterwalder J 2004 Boron nitride nanomesh *Science* **303** 217–20
- [7] Manzeli S, Ovchinnikov D, Pasquier D, Yazyev O V and Kis A 2017 2D transition metal dichalcogenides *Nat. Rev. Mater.* **2** 17033
- [8] Allen M J, Tung V C and Kaner R B 2010 Honeycomb carbon: a review of graphene *Chem. Rev.* **110** 132–45
- [9] Balandin A A, Ghosh S, Bao W, Calizo I, Teweldebrhan D, Miao F and Lau C N 2008 Superior thermal conductivity of single-layer graphene *Nano Lett.* **8** 902–7
- [10] Morozov S V, Novoselov K S, Katsnelson M I, Schedin F, Elias D C, Jaszczak J A and Geim A K 2008 Giant intrinsic carrier mobilities in graphene and its bilayer *Phys. Rev. Lett.* **100** 016602
- [11] Castro Neto A H, Guinea F, Peres N M R, Novoselov K S and Geim A K 2009 The electronic properties of graphene *Rev. Mod. Phys.* **81** 109–62

- [12] Blake P *et al* 2008 Graphene-based liquid crystal device *Nano Lett.* **8** 1704–8
- [13] Lee C, Wei X D, Kysar J W and Hone J 2008 Measurement of the elastic properties and intrinsic strength of monolayer graphene *Science* **321** 385–8
- [14] Wang X, Zhi L and Müllen K 2008 Transparent, conductive graphene electrodes for dye-sensitized solar cells *Nano Lett.* **8** 323–7
- [15] Bonaccorso F, Sun Z, Hasan T and Ferrari A C 2010 Graphene photonics and optoelectronics *Nat. Photonics* **4** 611–22
- [16] Zhao W, Gebhardt J, Späth F, Gotterbarm K, Gleichweit C, Steinrück H-P, Göring A and Papp C 2015 Reversible hydrogenation of graphene on Ni(111)—synthesis of ‘graphone’ *Chem. Eur. J.* **21** 3347–58
- [17] Wintterlin J and Bocquet M L 2009 Graphene on metal surfaces *Surf. Sci.* **603** 1841–52
- [18] Geim A K 2009 Graphene: status and prospects *Science* **324** 1530–4
- [19] Novoselov K S, Fal’ko V I, Colombo L, Gellert P R, Schwab M G and Kim K 2012 A roadmap for graphene *Nature* **490** 192–200
- [20] Whitener K E and Sheehan P E 2014 Graphene synthesis *Diam. Relat. Mater.* **46** 25–34
- [21] Dean C R *et al* 2010 Boron nitride substrates for high-quality graphene electronics *Nat. Nanotechnol.* **5** 722–6
- [22] Liu Z *et al* 2013 Ultrathin high-temperature oxidation-resistant coatings of hexagonal boron nitride *Nat. Commun.* **4** 2541
- [23] Li L H, Xing T, Chen Y and Jones R 2014 Boron nitride nanosheets for metal protection *Adv. Mater. Interfaces* **1** 1300132
- [24] Zhang K, Feng Y, Wang F, Yang Z and Wang J 2017 Two dimensional hexagonal boron nitride (2D-hBN): synthesis, properties and applications *J. Mater. Chem. C* **5** 11992–2022
- [25] Roy S *et al* 2021 Structure, properties and applications of two-dimensional hexagonal boron nitride *Adv. Mater.* **33** 2101589
- [26] Preobrajenski A B, Nesterov M A, Ng M L, Vinogradov A S and Mårtensson N 2007 Monolayer h-BN on lattice-mismatched metal surfaces: on the formation of the nanomesh *Chem. Phys. Lett.* **446** 119–23
- [27] Preobrajenski A B, Ng M L, Vinogradov A S and Mårtensson N 2008 Controlling graphene corrugation on lattice-mismatched substrates *Phys. Rev. B* **78** 073401
- [28] Voloshina E N, Dedkov Y S, Torbrügge S, Thissen A and Fonin M 2012 Graphene on Rh(111): scanning tunneling and atomic force microscopies studies *Appl. Phys. Lett.* **100** 241606
- [29] Gotterbarm K, Steiner C, Bronnbauer C, Bauer U, Steinrück H-P, Maier S and Papp C 2014 Graphene-templated growth of Pd nanoclusters *J. Phys. Chem. C* **118** 15934–9
- [30] Auwärter W 2019 Hexagonal boron nitride monolayers on metal supports: versatile templates for atoms, molecules and nanostructures *Surf. Sci. Rep.* **74** 1–95
- [31] Hummers W S and Offeman R E 1958 Preparation of graphitic oxide *J. Am. Chem. Soc.* **80** 1339
- [32] Hirsch A, Englert J M and Hauke F 2013 Wet chemical functionalization of graphene *Acc. Chem. Res.* **46** 87–96
- [33] Dai L 2013 Functionalization of graphene for efficient energy conversion and storage *Acc. Chem. Res.* **46** 31–42
- [34] Koch R J *et al* 2012 Growth and electronic structure of nitrogen-doped graphene on Ni(111) *Phys. Rev. B* **86** 075401
- [35] Gebhardt J *et al* 2013 Growth and electronic structure of boron-doped graphene *Phys. Rev. B* **87** 155437
- [36] Usachov D, Adamchuk V K, Haberer D, Grüneis A, Sachdev H, Preobrajenski A B, Laubschat C and Vyalikh D V 2010 Quasifreestanding single-layer hexagonal boron nitride as a substrate for graphene synthesis *Phys. Rev. B* **82** 075415
- [37] Grånäs E, Knudsen J, Schröder U A, Gerber T, Busse C, Arman M A, Schulte K, Andersen J N and Michely T 2012 Oxygen intercalation under graphene on Ir(111): energetics, kinetics, and the role of graphene edges *ACS Nano* **6** 9951–63
- [38] Balog R, Jørgensen B, Wells J, Lægsgaard E, Hofmann P, Besenbacher F and Hornekær L 2009 Atomic hydrogen adsorbate structures on graphene *J. Am. Chem. Soc.* **131** 8744–5
- [39] Vinogradov N A, Schulte K, Ng M L, Mikkelsen A, Lundgren E, Mårtensson N and Preobrajenski A B 2011 Impact of atomic oxygen on the structure of graphene formed on Ir(111) and Pt(111) *J. Phys. Chem. C* **115** 9568–77
- [40] Späth F, Gebhardt J, Düll F, Bauer U, Bachmann P, Gleichweit C, Göring A, Steinrück H-P and Papp C 2017 Hydrogenation and hydrogen intercalation of hexagonal boron nitride on Ni(111): reactivity and electronic structure *2D Mater.* **4** 035026
- [41] Späth F *et al* 2019 Oxygen functionalization of hexagonal boron nitride on Ni(111) *Chem. Eur. J.* **25** 8884–93
- [42] Freiberger E M *et al* 2021 Selective oxygen and hydrogen functionalization of the h-BN/Rh(111) nanomesh *Chem. Eur. J.* **27** 13172–80
- [43] Khan R, Nakagawa R, Campeon B and Nishina Y 2020 A simple and robust functionalization of graphene for advanced energy devices *ACS Appl. Mater. Interfaces* **12** 12736–42
- [44] Helmholtz-Zentrum Berlin für Materialien und Energie 2016 The plane grating monochromator beamline U49/2 PGM1 at BESSY II *JLSRF* **2** A72
- [45] Denecke R, Kinne M, Whelan C M and Steinrück H-P 2002 *In situ* core-level photoelectron spectroscopy of adsorbates on surfaces involving a molecular beam - General setup and first experiments *Surf. Rev. Lett.* **09** 797–801
- [46] Wideman T and Sneddon L G 1995 Convenient procedures for the laboratory preparation of borazine *Inorg. Chem.* **34** 1002–3
- [47] Laskowski R and Blaha P 2008 Unraveling the structure of the h-BN/Rh(111) nanomesh with *ab initio* calculations *J. Phys. Condens. Matter* **20** 064207
- [48] Kresse G and Furthmüller J 1996 Efficiency of *ab initio* total energy calculations for metals and semiconductors using a plane-wave basis set *Comput. Mater. Sci.* **6** 15–50
- [49] Kresse G and Furthmüller J 1996 Efficient iterative schemes for *ab initio* total-energy calculations using a plane-wave basis set *Phys. Rev.* **54** 11169–86
- [50] Kresse G and Joubert D 1999 From ultrasoft pseudopotentials to the projector augmented-wave method *Phys. Rev.* **59** 1758–75
- [51] Perdew J P, Burke K and Ernzerhof M 1996 Generalized gradient approximation made simple *Phys. Rev. Lett.* **77** 3865–8
- [52] Grimme S, Antony J, Ehrlich S and Krieg H 2010 A consistent and accurate *ab initio* parametrization of density functional dispersion correction (DFT-D) for the 94 elements H–Pu *J. Chem. Phys.* **132** 154104
- [53] Grimme S, Ehrlich S and Goerigk L 2011 Effect of the damping function in dispersion corrected density functional theory *J. Comput. Chem.* **32** 1456–65
- [54] McKee W C, Meunier V and Xu Y 2015 Reconciling the electronic and geometric corrugations of the hexagonal boron nitride and graphene nanomeshes *Surf. Sci.* **642** L16–9
- [55] Romero-Muñiz C, Martín-Recio A, Pou P, Gómez-Rodríguez J M and Pérez R 2016 Strong dependence

- of flattening and decoupling of graphene on metals on the local distribution of intercalated oxygen atoms *Carbon* **101** 129–34
- [56] Martín-Recio A, Romero-Muñiz C, Pou P, Pérez R and Gómez-Rodríguez J M 2018 Combining nitrogen substitutional defects and oxygen intercalation to control the graphene corrugation and doping level *Carbon* **130** 362–8
- [57] Romero-Muñiz C, Martín-Recio A, Pou P, Gómez-Rodríguez J M and Pérez R 2018 Unveiling the atomistic mechanisms for oxygen intercalation in a strongly interacting graphene–metal interface *Phys. Chem. Chem. Phys.* **20** 13370–8
- [58] Jiménez-Sánchez M D, Romero-Muñiz C, Pou P, Pérez R and Gómez-Rodríguez J M 2021 Graphene on Rh(111): a template for growing ordered arrays of metal nanoparticles with different periodicities *Carbon* **173** 1073–81
- [59] Methfessel M and Paxton A T 1989 High-precision sampling for Brillouin-zone integration in metals *Phys. Rev.* **40** 3616–21
- [60] Jinnouchi R, Lahnsteiner J, Karsai F, Kresse G and Bokdam M 2019 Phase transitions of hybrid perovskites simulated by machine-learning force fields trained on the fly with Bayesian inference *Phys. Rev. Lett.* **122** 225701
- [61] Jinnouchi R, Karsai F and Kresse G 2019 On-the-fly machine learning force field generation: application to melting points *Phys. Rev.* **100** 014105
- [62] Jinnouchi R, Karsai F, Verdi C, Asahi R and Kresse G 2020 Descriptors representing two- and three-body atomic distributions and their effects on the accuracy of machine-learned inter-atomic potentials *J. Chem. Phys.* **152** 234102
- [63] Soni H R, Gebhardt J and Görling A 2018 Reactivity of substrate-supported graphene: a case study of hydrogenation *J. Phys. Chem.* **122** 2761–72
- [64] Nosé S 1984 A unified formulation of the constant temperature molecular dynamics methods *J. Chem. Phys.* **81** 511–9
- [65] Düll F *et al* 2019 Growth and stability of Pt nanoclusters from 1 to 50 atoms on h-BN/Rh(111) *Phys. Chem. Chem. Phys.* **21** 21287–95
- [66] Schröder U A *et al* 2016 Core level shifts of intercalated graphene *2D Mater.* **4** 015013
- [67] Düll F, Freiberger E M, Bachmann P, Steinhauer J and Papp C 2019 Pt nanoclusters sandwiched between hexagonal boron nitride and nanographene as van der Waals heterostructures for optoelectronics *ACS Appl. Nano Mater.* **2** 7019–24
- [68] Svensson P H and Kloo L 2003 Synthesis, structure, and bonding in polyiodide and metal iodide–iodine systems *Chem. Rev.* **103** 1649–84
- [69] Chen X, Rickard M A, Hull J W, Zheng C, Leugers A and Simoncic P 2010 Raman spectroscopic investigation of tetraethylammonium polybromides *Inorg. Chem.* **49** 8684–9
- [70] Wu Y, Huang P-W, Howe J D, Yan Y, Martinez J, Marianchuk A, Zhang Y, Chen H and Liu N 2019 In operando visualization of the electrochemical formation of liquid polybromide microdroplets *Angew. Chem. Int. Ed.* **58** 15228–34
- [71] Jung N, Kim N, Jockusch S, Turro N J, Kim P and Brus L 2009 Charge transfer chemical doping of few layer graphenes: charge distribution and band gap formation *Nano Lett.* **9** 4133–7
- [72] Tristant D, Puech P and Gerber I C 2015 Theoretical study of polyiodide formation and stability on monolayer and bilayer graphene *Phys. Chem. Chem. Phys.* **17** 30045–51
- [73] Freiberger E M, Steffen J, Waleska-Wellnhofer N J, Harrer A, Hemauer F, Schwaab V, Görling A, Steinrück H-P and Papp C 2023 Bromine adsorption and thermal stability on Rh(111): a combined XPS, LEED and DFT study *ChemPhysChem* **24** e202300510
- [74] Düll F, Späth F, Bauer U, Bachmann P, Steinhauer J, Steinrück H-P and Papp C 2018 Reactivity of CO on sulfur-passivated graphene-supported platinum nanocluster arrays *J. Phys. Chem.* **122** 16008–15
- [75] Guo H, Ji W, Polanyi J C and Yang J 2008 Molecular dynamics of localized reaction, experiment and theory: methyl bromide on Si(111)-7 × 7 *ACS Nano* **2** 699–706
- [76] Huber V, Bikaljevic D, Redinger J and Memmel N 2016 Structure of low and high coverage phases of bromine on Pd(110) *J. Phys. Chem.* **120** 13523–30